Article

ACS APPLIED

POLYMER MATERIALS

# **Dual-Responsive Fluorescent Polymer Films for Wide-Range Temperature and Humidity Sensing**

Rayan Kadah El Habbal, Swapnil S. Salvi, Ankur Jain, and Pierre Karam\*



Cite This: https://doi.org/10.1021/acsapm.5c02854



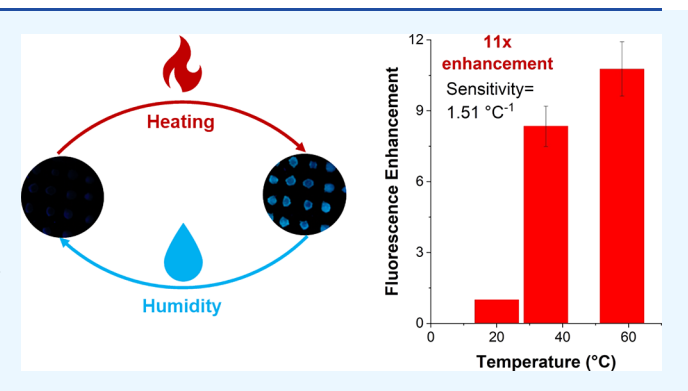
ACCESS I

III Metrics & More

Article Recommendations

s Supporting Information

ABSTRACT: Polymer films are widely used in packaging, electronics, and biomedical technologies. Preparing thin polymer films with temperature and humidity sensing capabilities can enable the improvement of device performance, durability, and functionality. In the present work, we report on thin fluorescent polymer films that can detect small temperature changes with excellent sensitivity over a wide temperature range from 20 to 60 °C. The probe was prepared using poly(phenylene ethylene) (PPE-CO<sub>2</sub>-108) in complexation with a polymer mixture of polyvinylpyrrolidone (PVP) and poly(1-vinylpyrrolidone-co-vinyl acetate) (PVP-VA). The macromolecule mixture resulted in clear and colorless films. Upon heating, we observed up to an 11-fold increase in the fluorescence intensity, which was recorded using an



unmodified and commercially available camera. The thermal response profile of these films could be tuned by altering the polymer composition and ratio. The best-performing films had an absolute sensitivity of 1.51 °C<sup>-1</sup>. The enhanced fluorescence signal was preserved even after several days of heat exposure; however, it would revert to its original intensity when exposed to humidity. As such, these prepared films can act as an on-off temperature sensor and as an on-off humidity sensor. ATR-FTIR measurements revealed that the actuating mechanism of the polymer films is through water adsorption-desorption in the polymer film. Fluorescence confocal imaging of the films before and after heating revealed a significant transformation in their morphology. Initially uniform, the films became highly porous upon heating, forming a distinct network-like structure. As a proof of concept, we demonstrated that these thermally sensitive films could serve as a valuable tool for investigating localized heating effects, such as the hyperthermia induced by magnetic nanoparticles embedded in thin polymer matrices.

KEYWORDS: poly(phenylene ethylene), poly(1-vinylpyrrolidone-co-vinyl acetate), Humidity sensing, Thermal sensing, Conjugated polyelectrolytes

#### INTRODUCTION

The measurement of humidity and temperature is critical in many fields of biomedicine, food production, energy conversion, and storage devices to ensure safety/reliability and maximize efficiency. Thin polymer films provide a technological advantage when probing these critical parameters since they can be printed into labels and optically monitored from a distance. For instance, heat dissipation plays a critical role in ensuring the performance and reliability of electronic devices.<sup>2,3</sup> Overheating in Li-ion cells is recognized to be a critical technological challenge that limits both performance and reliability. When the cell temperature exceeds a certain threshold, it may enter a thermally unstable state, which may eventually lead to explosions and/or fire. In high-performing aerodynamic machinery such as airplanes, aircraft, and racing cars, temperature-sensitive polymer films can be instrumental in monitoring overheating or thermal stress on surfaces exposed to high aerodynamic friction.<sup>6,7</sup> In addition to the ease of deployment, real-time data provided by such films may

enable early detection or prediction of potential failures in critical components. Hyperthermia is another example in which heat is generated by magnetic nanoparticles exposed to an alternating magnetic field.8 Gaining a fundamental understanding of this phenomenon is crucial for application in fields such as targeted drug delivery and cancer therapy. However, accurately measuring the localized temperature rise remains challenging, as conventional thermal sensing methods often fail. For example, the applied alternating magnetic field can induce heating in the thermal sensors themselves, compromising measurement accuracy.

Received: August 5, 2025 Revised: September 6, 2025 Accepted: September 14, 2025



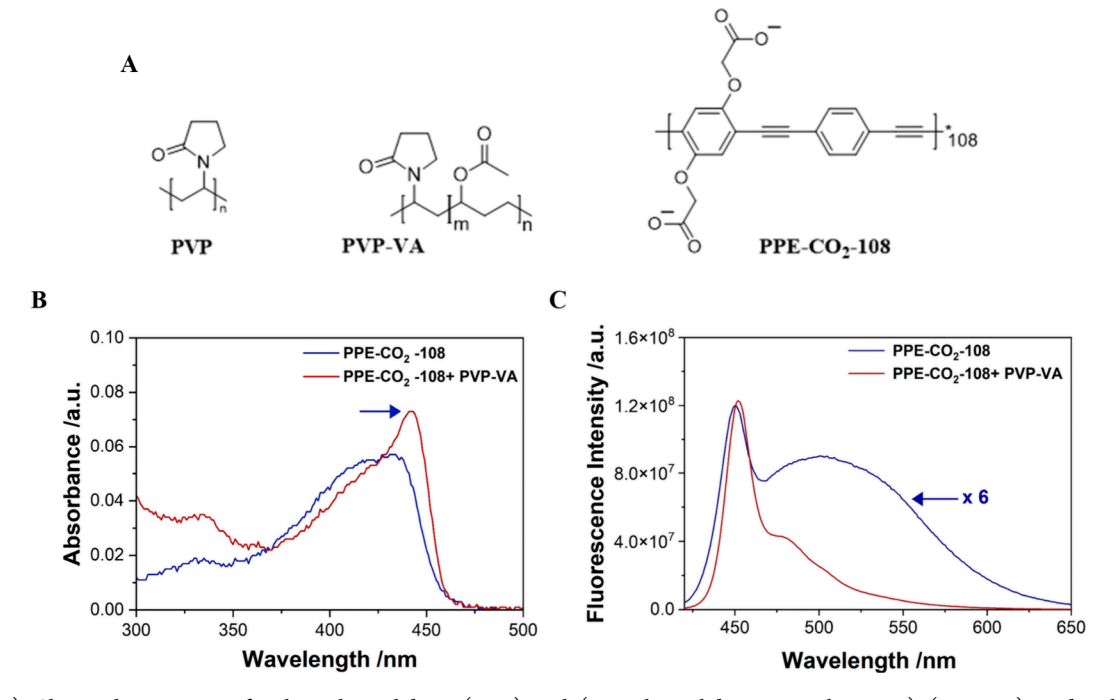


Figure 1. (A) Chemical structures of polyvinylpyrrolidone (PVP), poly(1-vinylpyrrolidone-co-vinyl acetate) (PVP-VA), and poly(phenylene ethynylene) PPE-CO<sub>2</sub>-108. (B) Absorption spectra of PPE-CO<sub>2</sub>-108 (5  $\mu$ g/mL) with PVP-VA (4.75 mg/mL) in deionized water. (C) Emission spectra of PPE-CO<sub>2</sub>-108 (5  $\mu$ g/mL) multiplied by 6 to facilitate its comparison to the emission upon the addition of PVP-VA (4.75 mg/mL) in deionized water.

A printable humidity sensor can provide real-time data about moisture levels, which can be beneficial for the packaging industry. For instance, food can be kept fresh during transport, and degradation of humidity-sensitive medicine can be prevented, ensuring quality and compliance with regulations. Humidity also plays a major role in the agricultural sector, especially in greenhouse management. Cheap, printable humidity sensors can prove instrumental when monitoring localized humidity conditions across a large field.

Optical-based sensors have been reported for the detection of temperature and humidity. For instance, Mach–Zehnder interferometers modified with graphene oxide or poly(vinyl alcohol) coating have reported sensitivities around 128 pm/% relative humidity (%RH). Fiber Bragg grating systems with polymer films demonstrate sensitivities of 94–231%RH. Luminescent temperature sensors using glutamine B or ruthenium complexes show intensity changes of 1.4 to 2.3% per  $^{\circ}$ C. Current systems often require complex optical setups and show moderate sensitivities, highlighting the need for simpler, more sensitive sensors.

We have worked extensively on developing thermal sensors based on conjugated polyelectrolytes (CPEs). <sup>18–20</sup> Specifically, we have developed one of the few reported examples of a thin-polymer film thermal sensor in our previous work. <sup>21</sup> Short poly(phenylene ethylene) (PPE-CO<sub>2</sub>-7), of an average of 7 monomers and Rhodamine were complexed with either poly(vinylpyrrolidone)-co-vinyl acetate (PVP-VA) or polyvinylpyrrolidone polystyrene (PVP-PS). The CPE-based film sensor showed a 3-fold increase in the fluorescence intensity when the temperature was raised to 50 °C. Since the publication of that work, we have learned how to tweak the PPE-CO<sub>2</sub> conjugated polymer environment to improve its response and tune its reversibility; specifically by using longer conjugated polyelectrolytes (PPE-CO<sub>2</sub>-108) and higher PVP

molecular weights. These new sensors, given their inherited steric hindrance, do not revert back to their original aggregated and less emissive state when heated. This has resulted in the development of thermal sensors with temperature memory, allowing the detection of the highest temperature that the sample was exposed to, even after cooling. More importantly, we have also learned the effect of the substrate on the photochemistry of the conjugated polymers. The previous sensor, prepared on a glass coverslip, could be used in diverse microscopic applications, but had somewhat limited thermal response. In the present study, we opted to use a more flexible substrate and one that would not affect the CPE thermal response dramatically.

In this work, we combine the thermal sensitivity of the PPE-CO<sub>2</sub>-108, which can be turned into thermal memory probes, together with the moisture-responsive actuation of polyvinylpyrrolidone (PVP) polymers, and the excellent thin-film forming properties and broad surface-binding affinity of PVP-VA (Figure 1.A). 22,23 This synergy between the properties of the macromolecules yields a dual response polymer sensor; an off-on response when the films are exposed to an increase in temperature and an on-off response when the films are exposed to an increase in humidity. Depending on the intended application, the films, under a controlled environment, can be reactivated by exposing them to high temperature and then humidity. Unlike our previous work, the reported polymer film sensors exhibit temperature memory properties with a tunable thermal response, higher sensitivity, and an improved dynamic range. Building on these enhanced properties, we demonstrated that the temperature rise induced by magnetic nanoparticles embedded within the thermal film when subjected to an alternating magnetic field can be accurately measured post-heating.

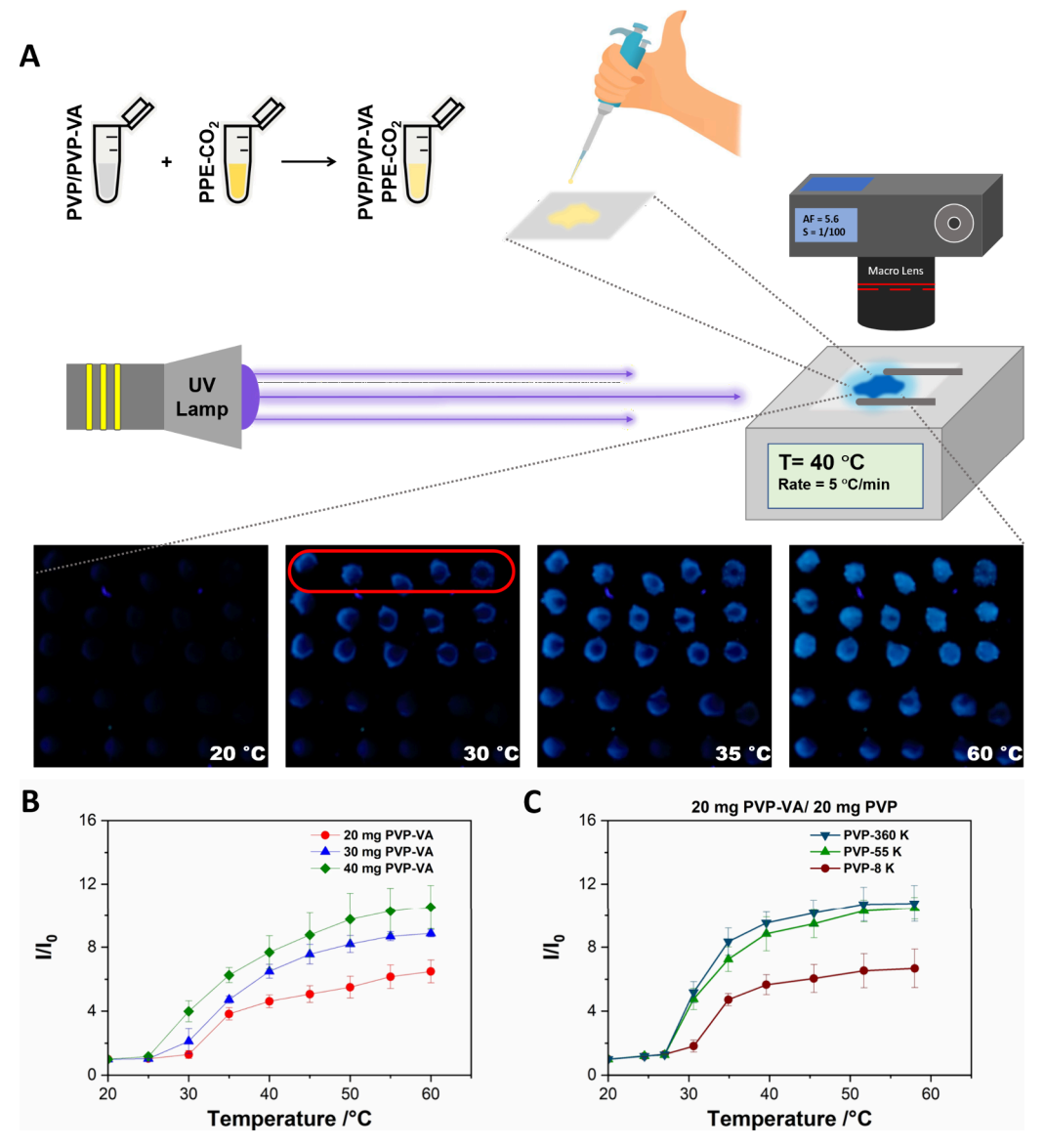


Figure 2. Schematic representation of the sample preparation and imaging setup used to assess the thermal response of the dried PVP-VA/PPE-CO $_2$ -108 polymer dots prepared on black duct tape. A UV lamp is used to excite the films, which are heated using a temperature control stage. The change in the emission intensity of the films with temperature increments of 5 °C is measured with a commercially available DSLR camera positioned above the films. Each horizontal series of samples represents different experimental conditions. Average thermal response extracted from the green channel ( $I_{green}$ ) of the polymer films prepared (B) from 20, 30, and 40 mg of PVP-VA when mixed with PPE-CO $_2$ -108 and (C) from 20 mg PVP-VA and 20 mg of different PVP molecular weights (8, 55, and 360 K) when mixed with PPE-CO $_2$ -108. The fluorescence intensity of the films was measured under UV between 20.0 and 60.0 °C; with a 5 °C increment.

## RESULTS AND DISCUSSION

This study is divided into four sections: we first optimized the off-on thermal response and the temperature memory properties of PVP-VA/PPE-CO<sub>2</sub>-108. We then assessed the effect of humidity on the fluorescence signal. We also carried out ATR-FTIR and fluorescent microscopy imaging analysis of these films to understand the actuating mechanism. Lastly, we demonstrated the ability of the thermal films to post-measure temperatures induced by hyperthermia.

Initially, we aimed to confirm the interaction between the long PPE-CO<sub>2</sub>-108 and the PVP-VA macromolecules. The absorption of pristine PPE-CO<sub>2</sub>-108 shows a maximum peak centered at 427 nm. Upon the addition of PVP-VA (4.75 mg/mL), we observed a 16 nm red shift, coupled with an increase in the relative intensity (Figure 1.B). This shift and increase in

intensity are indicative of strong interchain interactions, the extension in the average conjugation length, and the planarization of the poly(phenylene ethynylene) backbone. A similar change in the absorption was observed previously when PPE-based conjugated polyelectrolytes were studied with different side groups, coupled to other macromolecules, or prepared in different solvents. 25–27

Conjugated polyelectrolyte emission is highly dependent on its conformation and solvation state. Specifically, when dissolved in water, the stiff hydrophobic backbone of PPE-CO<sub>2</sub> tends to aggregate and emit from low-energy excimer-like species at around 520 nm. When well dissolved, the emission peak shifts to higher energies and emits at around 450 nm. This change in fluorescence emission allows us to engineer a sensing scheme that reports on external stimuli. When PPE-

CO<sub>2</sub>-108 and PVP-VA were mixed in aqueous solution, the measured changes in the fluorescence signal revealed strong interactions between the two polymers (Figure 1.C); we observed a 6 fold enhancement in the signal at 450 nm, suggesting efficient disaggregation of the PPE-CO<sub>2</sub>-108 polymer in the presence of PVP-VA. In addition, the broad structureless peak that was initially observed at 520 nm in the CPE solution disappeared completely. This shift in fluorescence intensity was observed when PPE-CO2 was mixed, for instance, with different types of lipid membranes.<sup>30</sup> Especially, when mixed with positively charged lipids, the fluorescence intensity shifted to 450 nm, and the structureless broad peak of the aggregated CPEs disappeared. The reverse trends were observed when well-dissolved PPE-CO<sub>2</sub> chains in methanol were aggregated in the presence of  $\mathrm{Ca^{2+}}^{.31}$  The addition of the divalent cation to the CPE chains led to a red shift in the fluorescence signal away from 450 nm, accompanied by a broadening in the peak, and a dramatic decrease in the overall intensity. As such, the obtained spectroscopic data confirmed a strong interaction between the two macromolecules in solution, leading to the molecular-level disaggregation of small conjugated polyelectrolytes chain aggregates. We expect that these interactions will translate well into the polymer films.

Thermal Response of PVP-VA/PPE-CO<sub>2</sub>-108 Films. Before assessing the thermal response of the PVP-VA/PPE-CO<sub>2</sub>-108, we looked for a substrate that is flexible, has no fluorescence background under UV light, and does not interfere with the fluorescence signal of our conjugated polymers. We tested many options (different regular papers, scotch tape, etc., Figure S.1), but we settled on using black duct tape. These tapes fulfilled all the aforementioned criteria and resulted in an excellent thermal response window.

Next, our objective was to establish the optimal ratio between PPE-CO<sub>2</sub>-108 and PVP-VA as thin polymer films to get the highest fluorescence enhancement with the increase in temperature. As such, we were guided by two criteria:

We wanted to ensure that the tested PPE-CO<sub>2</sub>-108:PVP-VA ratio would yield an initial fluorescence signal that is at least 10 standard deviations above the average background, thus providing a reliably detectable signal from the conjugated polyelectrolyte at room temperature (Figure S.2). It was found that reducing the ratio enhances the overall calculated fluorescence signal enhancement due to the low initial baseline value; however, this increased the risk of confusing the background signal from the true CPE signal. As such, the lowest PVP-VA mass to be used was determined to be at 20 mg.

We wanted to identify the optimal RGB color channel(s). To this end, the thin polymer films were analyzed using ImageJ to extract the intensities from the RGB channels. The green channel was identified as the best one to monitor, given its signal-to-background ratio and high responsiveness to changes in fluorescence intensity with temperature variations (Figure S.2).

Next, we tested the thermal response of films prepared using different initial amounts of PVP-VA upon exposure to temperature changes between 20.0 and 60.0 °C. Visually, a clear enhancement in the fluorescence signal was observed with the increase in temperature, going from an almost completely dark state to a bright blue color (Figure 2A). The fluorescence intensity increased initially, at the edges, and then

expanded to the entire dot with the increase in temperature. With the increase in the PVP-VA concentration, we observed an increase in the maximum fluorescence enhancement at 60  $^{\circ}$ C from 6.48  $\pm$  0.72 at 20 mg/mL to 10.56  $\pm$  0.33 at 40 mg/ mL (Figure 2B). In addition, we observed two distinct patterns influenced by changes in the polymer ratios. At the highest concentration of PVP-VA, the sensor film demonstrated greater responsiveness at lower temperatures, with an expanded dynamic range. Specifically, a fluorescence intensity increase was first detected at 30 °C, whereas no changes were observed before 35 °C at the lower PVP-VA concentration (20 mg/mL). Moreover, a wider dynamic range, extending up to 60 °C was observed at 40 mg/mL PVP-VA. We then calculated the absolute thermal sensitivity by calculating the slope of the best-fit curves. The three tested films exhibited good sensitivity with the 30 and 40 mg, showing a steady decrease with the increase in temperature (Figure S3A). However, with the 20 mg PVP-VA films, the highest thermal sensitivity was observed only within a narrow temperature range before rapidly decreasing and plateauing at around 35 °C.

These findings suggest that adjusting the concentration of PVP-VA allows for tuning of both the thermal response profile and sensitivity. We speculated that the observed effect is driven by a shift in the hydration state of those films.<sup>32</sup> The relative humidity was shown to affect the glass-transition temperature of PVP-VA.<sup>33</sup> These structural changes can, in turn, have an effect on the photophysics of the trapped conjugated polyelectrolytes.

Thermal Response of PVP/PVP-VA/PPE-CO<sub>2</sub>-108. Based on the previous results, we aimed to enhance the overall thermal response of the polymer films by introducing PVP of different molecular weights (8K, 55K, and 360 K). PVP is a hydrophilic polymer known for its exceptional wateradsorption capacity due to its polar amide groups, which readily form hydrogen bonds with water molecules. We argued that a higher PVP content may influence the thermal sensitivity of the film by modulating its hydration. We chose to mix PVP with 20 mg PVP-VA, given its higher initial thermal sensitivity with the aim to extend these values to higher temperatures. We observed that as the PVP molecular weight increased, the maximum fluorescence intensity increased (Figure 2C). Simultaneously, the temperature at which the fluorescence intensity began to rise shifted to lower values. For instance, when heated to 60 °C, the signal displayed a significant increase in intensity with the highest PVP molecular weight (MW = 360 K g/mol) reaching a total fluorescence enhancement of  $10.77 \pm 1.15$ . The dynamic window also increased, and the thermal response started from 27.5 °C. The addition of PVP also improved the absolute thermal sensitivity. In the absence of PVP, it dipped below 0.3 °C¹-at 33 °C, but it was extended to 37.5 °C with the addition of 360 K and 55K PVP. The maximum relative sensitivity was calculated to be  $118\%^{\circ}C^{1-}$  and  $94\%^{\circ}C^{1-}$  at  $27~^{\circ}C$  for the PVP-VA films prepared with PVP-360 K and 55K, respectively, and 70%°C1-, at 30 °C for the PVP-VA films prepared with PVP-8K (Figure S3 B). Despite maintaining a constant weight concentration, the dependence of the fluorescence enhancement on the PVP molecular weight indicates that a higher molecular weight exhibits a stronger interaction with the conjugated polyelectrolytes. Also, this observation is in line with previously reported findings where we showed that larger PVP molecular weight is better at stabilizing the disaggregated PPE-CO<sub>2</sub>-108, allowing greater solubilization/stabilization.<sup>34</sup> In addition,

higher molecular weight PVP with its larger hydrodynamic volume may produce a favorable microenvironment for the PPE-CO<sub>2</sub> by providing enhanced solvation/hydration or favorable microviscosity.<sup>35,36</sup> The interaction between PVP and water molecules was studied using X-ray diffraction, which revealed that water molecules first occupy the void spaces created by the PVP molecules before interacting with the polymer's backbone.<sup>37</sup> The increased void spaces created by the higher PVP molecular weight may be behind the improved thermal response. The higher PVP MW was also shown to result in a membrane with higher porosity and water retention.<sup>38</sup>

The thermal sensitivity (absolute =  $1.51 \, ^{\circ}\text{C}^{1-}$  and maximum relative sensitivity = 118% °C<sup>1-</sup>) of the best performing PVP-360 K/PVP-VA/PPE-CO<sub>2</sub>-108 film is much better than our previously reported thin film thermal sensor (PVP-VA/PPE- $CO_2$ -7/Rhodamine with absolute sensitivity of 0.01 °C<sup>1-</sup>)<sup>21</sup> and its relative sensitivity is better than previously reported thin film thermal sensors. For instance, using a digital camera, similar to our reported detection scheme, N,N-bis(2,5ditertbutylphenyl)-3,4,9,10-perylenedi carboximide-doped polystyrene films were reported with an absolute sensitivity of 0.0013 °C1-.39 Electrospun carbon nanofibers showed a relative sensitivity of 1.52% °C1- between 30 and 55 °C.40 Dysprosium-doped Gadolinium-Vanadate thin films were prepared with a reported absolute sensitivity of  $4 \times 10^{-3}$  and a relative sensitivity of 2% C<sup>-1</sup>. A single monoclinic phase of Mn<sup>4+</sup>-doped Sr<sub>2</sub>InTaO<sub>6</sub> phosphors was reported with a maximum relative sensitivity value of 3.27% C<sup>-1</sup> at 373 K.<sup>42</sup> Using lanthanide-based thermal sensitive thin films, a europium complex had a reported maximum relative sensitivity of 4% C<sup>-1</sup> at 290 K.<sup>43</sup> A thin film gold thermistor showed an absolute thermal sensitivity of  $3.03 \times 10^{-3}$  °C<sup>1-</sup> between 20-100 °C.44

Assessing the Thermal Memory Properties of PVP-360 K/PVP-VA/PPE-CO<sub>2</sub>-108. Next, we studied the temperature memory properties of the PVP-360 K/PVP-VA/PPE-CO<sub>2</sub>-108. Long-term measurements and retention of the heatinduced enhanced fluorescence signal are important for a variety of applications, such as micro/nanoelectronic devices, where mapping the heat dissipation may help optimize device performance. Heat dissipation plays a major role in electronic device performance.<sup>45</sup> It can affect the electrical conductivity and other key parameters, which can induce signal distortion. A nonuniform heat dissipation can also increase the thermal stress on the device, resulting in reduced lifespan and reliability. Another timely example, especially with the rapid adoption of electric cars, is the monitoring and understanding of thermal runaway in lithium-ion cells and battery packs. Excessive temperature rise in Li-ion cells reduces performance and also imposes a severe risk of uncontrolled thermal runaway, leading to fire.46

In order to understand and assess its thermal retention, PVP-360 K/PVP-VA/PPE-CO<sub>2</sub>-108 polymer films were heated to 60.0 °C for 3 min, cooled down to 20 °C, and then the signal was recorded at different time intervals (1 h, 2 h, 3 h, 4 h, 5 h, 6 h, 24 and 48 h) (Figure 3) under controlled environment. The reported intensity was normalized to the intensity recorded at 60 °C. The fluorescence intensity remained relatively constant over 48 h. As such, this approach allows temperature variation to be determined retrospectively when real-time/in situ measurements are unfeasible.

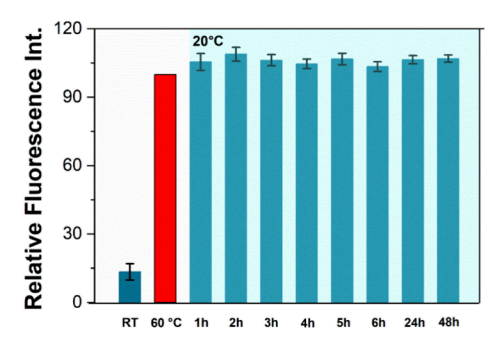


**Figure 3.** Relative intensity of the PVP-360 K/PVP-VA/PPE-CO $_2$ -108 polymer films once heated to 60  $^{\circ}$ C and then cooled down to 20  $^{\circ}$ C. The films were imaged under UV light, and the intensity from the green channel was monitored for 48 h at different time intervals to assess thermal memory. All relative intensities are normalized to the one measured at 60  $^{\circ}$ C.

Response to Changes in Humidity in the Activated PVP-360 K/PVP-VA/PPE-CO<sub>2</sub>-108 Films. A well-monitored humidity environment is also important for many applications. 47-49 The design of the reported films, integrating a hydrophilic polymer, enabled the synergistic sensing properties in our films. In addition to sensing changes in the temperature, the absorption of water when exposed to a high-humidity environment is expected to affect the PPE-CO2 photochemistry. PVP is frequently used for the preparation of a humidity sensor.<sup>50</sup> Its polar group exhibits hydrophilic properties, which make it excellent for sensing humidity.5 Once activated, upon exposure to 60 °C for a few minutes, the thin film probe became an on-off humidity sensor, which reverted back to its initial state when in a saturated humidity chamber. For instance, when the films were exposed to a 97% humidity environment for 20 min, the green intensity would reverse back (Figure 4.A). The intensity decreased to 5.89% ± 1.68% from its high of 100%. The samples were cycled again and reheated to 60 °C. Consequently, the intensity increased back again to 124.39%  $\pm$  5.54%. When the PVP/PVP-VA/ PPE-CO<sub>3</sub>-108 films are exposed to humidity, water molecules rehydrate those films, leading to a reversal in the fluorescence enhancement. The response of the activated films was evaluated under different relative humidity environments obtained by preparing different saturated salt solutions (Figure 4.B). The detection of humidity through the change in optical properties of these films opens avenues for applications in moisture detection in various fields, including food safety and environmental monitoring.

ATR-FTIR Analysis of Structural Changes Induced by Heat and Humidity. To gain an insight into the changes at the molecular level in the PVP-360 K/PVP-VA/PPE-CO<sub>2</sub>-108 film, we acquired ATR-FTIR spectra when films were heated and then exposed to humidity (Figure 5). The key observation in these measurements was a shift in the wavenumber for the functional groups that are usually involved in hydrogen bonding. For instance, the broad O-H stretching band shifts from 3431 to 3368 cm<sup>-1</sup> upon exposure to humidity, and its intensity increases dramatically (Figure S 4A and B). These observations are the result of the hydrogen bonding of the absorbed water molecules and the polymer lactam groups. In addition, the amide C = O stretch of the PVP lactam and the acetylene C = O also decrease from 1653 to 1639 cm<sup>-1</sup> and from 1731 to 1715 cm<sup>-1</sup> (Figure S 4C) as a result of the hydrogen bonding<sup>52</sup> In addition, the water uptake is confirmed

**ACS Applied Polymer Materials** 

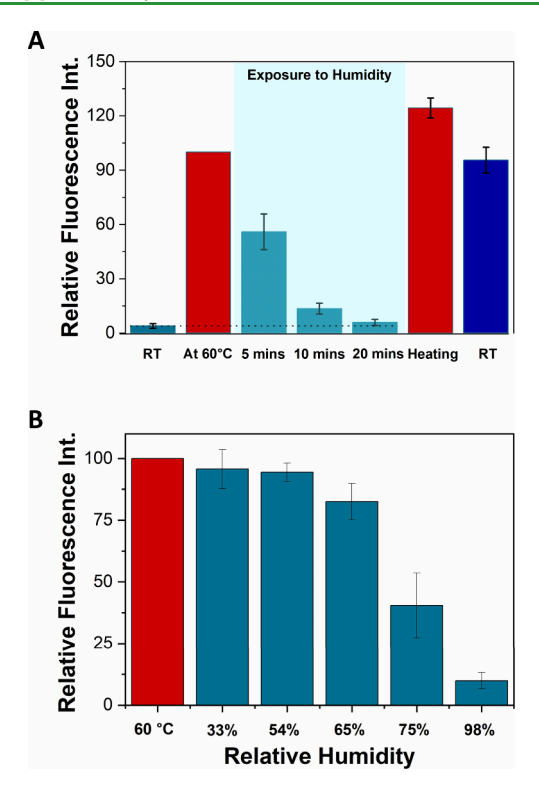


**Figure 4.** (A) Thermal response of the PVP-360 K/PVP-VA/PPE-CO $_2$ -108 polymer films once heated to 60 °C, cooled down to 20 °C, and then exposed to humidity at different time intervals. The films are then cycled back again by heating them again to 60 °C and then cooling them back to room temperature. (B) Fluorescence changes upon exposure to different relative humidity.

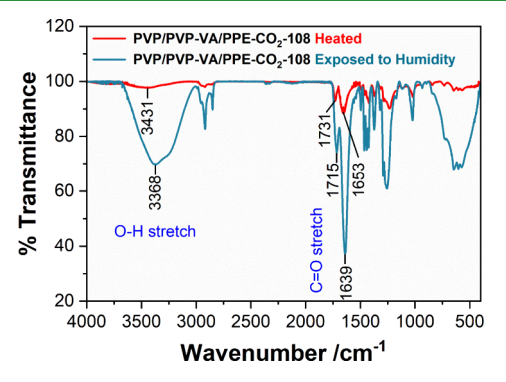


**Figure 5.** ATR-FTIR spectra of PVP-360 K/PVP-VA/PPE-CO2-108 after heating and exposure to humidity.

through a marked increase in the O–H stretching band around 3300 cm<sup>-1</sup>. Under humidity, the transmittance at this band decreased to 69%, compared to 97% when heated. When normalized against the C–H stretching band at 2900 cm<sup>-1</sup>, the O–H to C–H ratio increased from 1.00 (heated) to 1.71 (humidity).

Confocal Fluorescence Microscopy of Polymer Films Before and After Heating. Confocal fluorescence imaging microscopy was performed on the prepared films before and after heating. Initially, the polymer film exhibited a homogeneous structure with a monolithic appearance (Figure 6A). The surface morphology displayed circular depressions, resembling craters. These features are likely attributed to solvent evaporation-induced dewetting during film formation. 3D fluorescence images confirmed that these depressions are

superficial and do not extend to the underlying glass substrate (SI Movie I). Upon heating, the film surface became markedly more irregular. Exhibiting increased texture, granular roughness, and patterns indicative of heat-induced molecular rearrangement (Figure 6B). The 3D fluorescence images showed that the previously uniform structure had transformed into a porous, network-like morphology (SI Movie II). Fluorescence lifetime mapping revealed a shift toward longer lifetimes with the increase in temperature (Figure 6C and D), indicating a suppression in the nonradiative pathways. Ordered domains reduce structural disorder, such as torsional, resulting in reduced nonradiative pathways. Silva et al. have reported an enhancement in the fluorescent signal and suppression in the nonradiative decay when conjugated polymer chains with where aligned in a J-type coupling.<sup>53</sup> Similar behavior was observed under solvation annealing conditions.<sup>54</sup> More specifically, Swager et al. reported that upon alignment of PPE chains in liquid crystals, an increase in photoluminescence and a reduction in nonradiative decay pathways were observed.55,56

Fluorescence Emission Analysis of Polymer Films before and after Heating. Emission spectra from the prepared films were measured (Figure 6E). The freshly prepared films exhibited a maximum emission at 450 nm, which is indicative of the emission of disaggregated single PPE-CO<sub>2</sub> chains. In striking contrast, the emission of the heated films showed two distinct peaks. The first peak, centered at 460 nm, corresponds to the 0–0 transition, while the second, more intense peak at around 486 nm is attributed to the 0-1 vibronic transition. The quenching of the 0-0 band in the emission could be the result of major conformation changes in the conjugated polyelectrolyte chains from their solution form. The 486 nm peak is observed in solution when the PPE-CO<sub>2</sub>-7 polymer is slightly disaggregated in a mixture of polar and nonpolar solvents, and when an amphiphilic polymer is added, which helps destabilize the highly aggregated chains in water.<sup>57,58</sup> A similar observation was reported in thin films when poly(phenylene ethynylenes) was spun cast into thin films. A quenching in the 0-0 transition was attributed to the efficient interaction between the polymer backbones due to the high degree of alignment and increased planarization and strong  $\pi - \pi$  interchain interaction in a three-dimensional topology, increasing the efficiency of energy transfer to lowenergy traps. 59,60 These results complement the microscope images shown in Figures 6A-6D, which revealed a clear restructuring of the films and evidence for film drying and forming a network-like structure, which would induce the structural changes responsible for the observed spectroscopic changes.

Taken together, these results provide a robust mechanistic explanation for the observed increase in the fluorescence intensity. As the water molecules escape the films, the restructuring of the conjugated polymers decreases the nonradiative and increases the fluorescence intensity (Figure 6F).

Monitoring Local Heating of Magnetic Nanoparticles in Polymer Films. As a proof of concept, we demonstrate that the temperature memory system can report the maximum temperature of magnetic nanoparticles (MNPs) when embedded in polymer films and placed in an alternating magnetic field (AMF). In a phenomenon referred to as hyperthermia, <sup>61</sup> MNPs generate heat when placed in an AMF, which has been proven to be effective in inducing local

**ACS Applied Polymer Materials** 

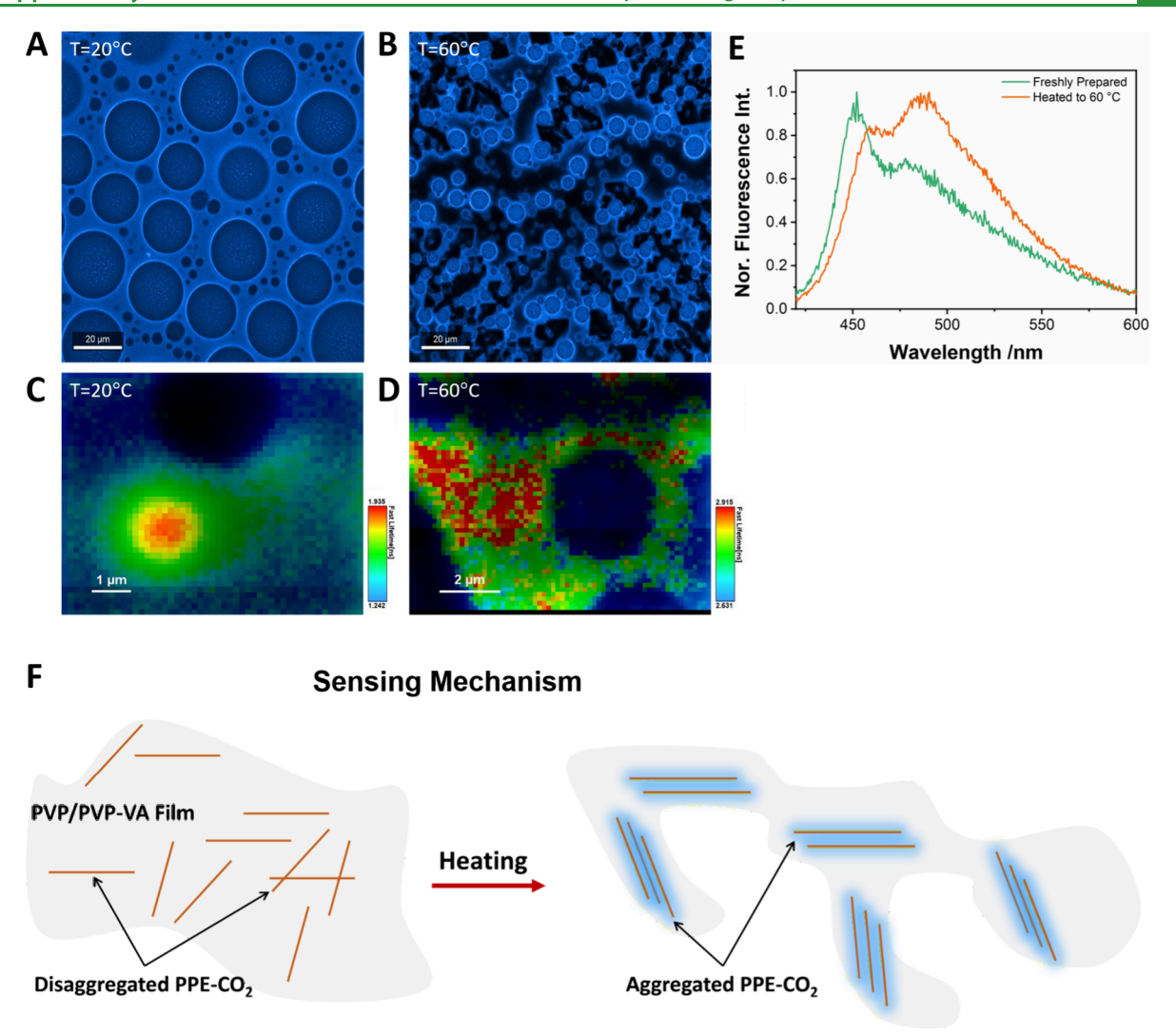


Figure 6. Fluorescence confocal microscopy images of PVP-360 K/PPE- $CO_2$ /PVP-VA films (A) before and (B) after heating, showing morphological transformation from a uniform film to a porous, network-like structure upon heating. Fluorescence lifetime microscopy images of the films (C) before and (D) after heating. (E) Fluorescence emission spectra of the films before and after heating. (F) Schematic illustration of the proposed mechanisms underlying the fluorescence enhancement.

catalytic reactions<sup>62</sup> and as a therapeutic strategy for cancer.<sup>63</sup> For instance, MNPs embedded in nanofibers of polycaprolactone and magnetic nanoparticles hydrogel showed significant heating and chemotherapeutic effects.<sup>64</sup>

However, unravelling the heating mechanism of hyperthermia remains challenging, especially in films where heating is expected to be different due to the limited Brownian motion. The most suitable thermal sensing techniques for in situ measurements for the aforementioned locally generated heat are fluorescence-based sensors. However, practically speaking, it is challenging to couple an alternating frequency generator with a fluorometer or a fluorescent microscope for in situ monitoring. The alternating magnetic field induces heating in the optical devices, causing interference if not permanent damage. In films, thermal measurements become even more challenging since using thermocouples — the method of choice for in-solution thermal monitoring — cannot capture the heterogeneity of films and lacks the required spatial resolution.

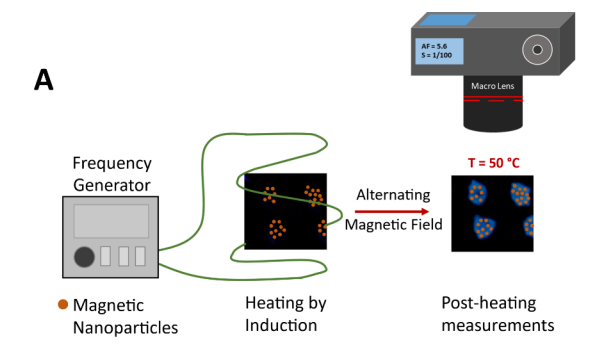
PVP-360 K/PVP-VA/PPE-CO<sub>2</sub>-108 films were prepared with different amounts of magnetic nanoparticles (0.4, 0.8, and 4.0  $\mu$ g of Fe<sub>3</sub>O<sub>4</sub>) (Figure 7A). The films were dried and then placed in an alternating magnetic field. After 1 h, the

fluorescence emission of the films was recorded, and the maximum temperature was calculated using the calibration curve reported in Figure 2. The films that contained the least amount of magnetic nanoparticles (0.4  $\mu$ g) showed the highest temperature increase (60 °C) (Figure 7B). This could be explained by the tendency of the magnetic nanoparticles to aggregate at higher concentrations, which would limit their hyperthermia efficiency. For instance, Guibert et al. reported a significant decrease in the specific loss power with the formation of large and dense aggregates of magnetic nanoparticles.  $^{65}$ 

This proof-of-concept is a great example of the experimental challenges that this temperature memory system can address, in scenarios where in situ thermal measurements are critical but practically not possible, especially when coupled with other techniques.

# CONCLUSIONS

In this work, we successfully developed a dual response fluorescence-based sensor for the detection of temperature and humidity. The PVP-360 K/PVP-VA/PPE-CO<sub>2</sub>-108 films



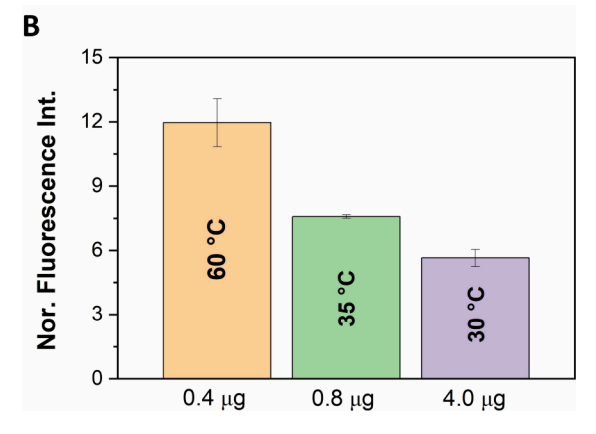


Figure 7. (A) Schematic of the magnetic nanoparticle hyperthermia heating measurement setup in PVP-360 K/PVP-VA/PPE-CO<sub>2</sub>-108 polymer films. (B) Calculated maximum temperature reached by magnetic nanoparticles after 1 h of being placed in an alternating magnetic field based on the recorded fluorescence enhancement of the thermally sensitive films at varying loads of magnetic nanoparticles.

exhibited fluorescence intensity changes measurable using a standard, unmodified camera. The fluorescence enhancement was preserved for at least 48 h after the films were heated. The films also demonstrated clear responsiveness to changes in humidity. A proof-of-concept experiment highlighted the sensor's potential for capturing thermal changes in contexts where conventional methods are impractical, such as in the presence of alternating magnetic fields. The reported sensor may therefore prove instrumental in the detection of thermal fluctuations in microelectronic devices, for instance, as well as in monitoring real-time humidity changes.

## MATERIALS AND METHODS

Materials. Microscope cover glasses (22 × 22 mm) were purchased from OMEGALAB, and the black duct tape from X-Fasten. We used poly(phenylene ethynylene) carboxylate (PPE-CO<sub>2</sub>-108), with an average of 108 monomer repeating units, which was synthesized as previously described. Polyvinylpyrrolidone (PVP) with different molecular weights (8K, 55K and 360 K) and N-(2-Hydroxyethyl) piperazine-N'-(2-ethanesulfonic acid) (HEPES) 1 M, Poly(1-vinylpyrrolidone-co-vinyl acetate) average MW 50 000 (PVP-VA), Iron(III) chloride hexahydrate (97%), anhydrous iron(II) chloride (98%), ammonium hydroxide (28–30%) and sodium citrate dihydrate (≥99%)were purchased from Sigma-Aldrich. Deionized water (18.2 MΩ-cm) was used in solution preparation.

**Spectroscopic Measurements.** The absorption spectra were measured using a Jasco V-570 UV/vis/NIR Spectrophotometer (double beam mode), and the steady-state fluorescence spectroscopy measurements were done using a Horiba Fluorolog-3 fluorometer.

The solutions were excited at 405 nm while collecting the emissions between 420 and 650 nm at room temperature.

Assessing the Thermal Response of the Polymer Films. The thermal sensing films were prepared by mixing 0.004 mg PPE-CO<sub>2</sub>-108 with 20 mg PVP of different molecular weights (3500, 8K, 55K, and 360 K), and 20 mg PVP-VA (MW 50k) in a buffer of 10 mM HEPES and 150 mM NaCl (pH = 7.3). To make the small polymer dot film, 5  $\mu$ L of the solution mixture is pipetted and dropped onto the black duct tape affixed to a coverslip. The solution was dried for 16 h before imaging. To study their thermal properties, polymer dots were heated using a temperature-controlled stage (Linkam LTS-120), and the temperature was increased to 60 °C with 5 °C increments. At each temperature, the film was imaged under UV light, using a Canon DSLR 750D Camera. At each increment, the films were kept for 3 min to stabilize their temperature. The intensities of the red, green, and blue color components were then analyzed using ImageJ. To assess the response of the prepared films under different humidity environments, we prepared saturated solutions of MgCl<sub>2</sub> 33% RH, Mg(NO<sub>3</sub>)<sub>2</sub> 54% RH, NaNO<sub>2</sub> 65% RH, NaCl 75% RH, and K<sub>2</sub>SO<sub>4</sub> 98% RH to establish a specific relative humidity in a sealed container.

Attenuated Total Reflectance Fourier Transform Infrared (ATR-FTIR) Spectroscopy. Fourier-transform Infrared (FTIR) Attenuated Total Reflectance (ATR) spectroscopy was measured on a Netzsch (F1 Libra). The FTIR spectra were taken between 4000 and 400 cm<sup>-1</sup> with a resolution of 1 cm<sup>-1</sup>. The reported spectra are the results of averaging 64 scans. The dried films were placed in a saturated humidity chamber for 10 min before subsequently measuring the spectra again.

**Preparation of Citrate-Iron Oxide NPs (MNPs).** For the preparation of magnetic nanoparticles (Fe $_3$ O $_4$ ), FeCl $_3$ ·6H $_2$ O and anhydrous FeCl $_2$  were mixed in deionized water under a nitrogen atmosphere and mechanical stirring, to achieve respective concentrations of 0.15 and 0.075 M. $^{67}$  Following this, a 1.6 M solution of ammonium hydroxide (28–30%) was added dropwise. Before adding sodium citrate dihydrate (at a final concentration of 0.17 M), the mixture was stirred for 30 min. To get rid of excess ammonium hydroxide, this reaction was then exposed to a water bath at a temperature of 90 °C and left for 45 min. Using a magnetic-assisted separation method, the nanoparticles were collected from the solution and purified using ethanol and acetone, followed by overnight drying. They were dispersed in deionized water. Lastly, to get rid of larger particles, a centrifugation at 4500 rpm was performed for 30 min.

Heating Using Alternating Magnetic Field (AMF). PVP-360 K/PVP-VA/PPE-CO<sub>2</sub>-108 films were prepared with different amounts of magnetic nanoparticles (0.4, 0.8, and 4.0  $\mu$ g of Fe<sub>3</sub>O<sub>4</sub>). The films were dried and then placed in an alternating magnetic field (NanoTherics MagneTherm) at a 109.6 kHz frequency. The voltage was set between 30 and 32 V. After 1 h, the fluorescence intensity of the films was recorded under UV light using a DSLR camera.

## ASSOCIATED CONTENT

#### Supporting Information

The Supporting Information is available free of charge at https://pubs.acs.org/doi/10.1021/acsapm.5c02854.

Additional characterization measurements (PDF)

3D fluorescence images confirming that the depressions are superficial and do not extend to the underlying glass substrate (MP4)

3D fluorescence images showing that the previously uniform structure had transformed into a porous, network-like morphology (MP4)

#### AUTHOR INFORMATION

#### **Corresponding Author**

Pierre Karam – Department of Chemistry, American University of Beirut, Beirut 1107 2020, Lebanon; orcid.org/0000-0003-4550-7641; Email: pierre.karam@aub.edu.lb

#### **Authors**

Rayan Kadah El Habbal – Department of Chemistry, American University of Beirut, Beirut 1107 2020, Lebanon; orcid.org/0000-0002-4861-1391

Swapnil S. Salvi — Department of Mechanical and Aerospace Engineering, The University of Texas at Arlington, Arlington, Texas 76019, United States

Ankur Jain — Department of Mechanical and Aerospace Engineering, The University of Texas at Arlington, Arlington, Texas 76019, United States

Complete contact information is available at: https://pubs.acs.org/10.1021/acsapm.5c02854

#### **Notes**

The authors declare no competing financial interest.

## ACKNOWLEDGMENTS

This work was supported by the University Research Board (#104391). The authors are also thankful to the Kamal A. Shair Central Research Science Lab (KAS CRSL) of the Faculty of Arts and Sciences at AUB for providing access to their facilities. P.K. is grateful to the Arab Fund Fellowships Program, the Trilateral Research Group Linkages from the Humboldt Foundation, and the Arab-American Frontiers Fellowship by the U.S. National Academy of Science.

#### REFERENCES

- (1) Cai, T.; Yan, Y.-Z.; Park, Y.; Lee, T.; Peng, D.; Liu, Y.; Ha, C.-S.; Kim, K. C. Phosphorescence-based flexible and transparent optical temperature-sensing skin capable of operating in extreme environments. ACS Applied Polymer Materials 2021, 3 (5), 2461–2469.
- (2) Salvi, S. S.; Jain, A. A review of recent research on heat transfer in three-dimensional integrated circuits (3-D ICs). *IEEE Transactions on Components, Packaging and Manufacturing Technology* **2021**, *11* (5), 802–821.
- (3) Fang, R.; Li, X.; Khan, S. A.; Wang, Z.; Cui, X.; Zhang, H.; Lin, Z.-H. Anhydrous Thermogalvanic Gel for Simultaneous Waste Heat Recovery and Thermal Management of Electronics. *ACS Applied Polymer Materials* **2023**, 5 (7), 4628–4635.
- (4) Shah, K.; Vishwakarma, V.; Jain, A. Measurement of multiscale thermal transport phenomena in Li-ion cells: A review. *J. Electrochem. Energy Convers. Storage* **2016**, *13* (3), No. 030801.
- (5) Mishra, D.; Jain, A. Multi-Mode Heat Transfer Simulations of the Onset and Propagation of Thermal Runaway in a Pack of Cylindrical Li-Ion Cells. *J. Electrochem. Soc.* **2021**, *168* (2), No. 020504.
- (6) Kumar, V.; Larsson, J. Modular method for estimation of velocity and temperature profiles in high-speed boundary layers. *AIAA J.* **2022**, 60 (9), 5165–5172.
- (7) Sommer, S. C.; Short, B. J.Free-flight measurements of turbulent-boundary-layer skin friction in the presence of severe aerodynamic heating at Mach numbers from 2.8 to 7.0; NACA 1955.
- (8) Deatsch, A. E.; Evans, E. E. Heating efficiency in magnetic nanoparticle hyperthermia. *J. Magn. Magn. Mater.* **2014**, 354, 163–172.
- (9) Kobayashi, T. Cancer hyperthermia using magnetic nanoparticles. *Biotechnology journal* **2011**, *6* (11), 1342–1347.
- (10) Tannarana, M.; Pataniya, P. M.; Bhakhar, S. A.; Solanki, G.; Valand, J.; Narayan, S.; Patel, K. D.; Jha, P. K.; Pathak, V. Humidity sensor based on two-dimensional SnSe2/MWCNT nanohybrids for the online monitoring of human respiration and a touchless positioning interface. ACS Sustainable Chem. Eng. 2020, 8 (33), 12595–12602.

- (11) Zhou, G.; Byun, J.-H.; Oh, Y.; Jung, B.-M.; Cha, H.-J.; Seong, D.-G.; Um, M.-K.; Hyun, S.; Chou, T.-W. Highly sensitive wearable textile-based humidity sensor made of high-strength, single-walled carbon nanotube/poly (vinyl alcohol) filaments. ACS Appl. Mater. Interfaces 2017, 9 (5), 4788–4797.
- (12) Dai, J.; Xie, G.; Chen, C.; Liu, Y.; Tai, H.; Jiang, Y.; Su, Y. Hierarchical piezoelectric composite film for self-powered moisture detection and wearable biomonitoring. *Appl. Phys. Lett.* **2024**, *124* (5), No. 053701.
- (13) Young, P. M.; Price, R.; Tobyn, M. J.; Buttrum, M.; Dey, F. The influence of relative humidity on the cohesion properties of micronized drugs used in inhalation therapy. *Journal of pharmaceutical sciences* **2004**, *93* (3), 753–761.
- (14) Mahmood, M. H.; Sultan, M.; Miyazaki, T. Significance of temperature and humidity control for agricultural products storage: overview of conventional and advanced options. *Int. J. Food Eng.* **2019**, *15* (10), 20190063.
- (15) Li, J.-x.; Tong, Z.-r.; Jing, L.; Zhang, W.-h.; Qin, J.; Liu, J.-w. Fiber temperature and humidity sensor based on photonic crystal fiber coated with graphene oxide. *Opt. Commun.* **2020**, 467, No. 125707.
- (16) Han, Z.; Chao, J.; Xiping, Z.; Pei, W.; Tingshui, C.; Changning, L.; Simei, S. Simultaneous humidity and temperature measurement sensor based on two cascaded long-period fiber gratings. *Opt. Commun.* **2023**, 530, No. 129137.
- (17) Gallery, J.; Gouterman, M.; Callis, J.; Khalil, G.; McLachlan, B.; Bell, J. Luminescent thermometry for aerodynamic measurements. *Review of scientific instruments* **1994**, *65* (3), 712–720.
- (18) Alhafi, K.; Merhi, N.; Karam, P. Single Particle Insights into the Thermal Sensing of Conjugated Polyelectrolyte-Nanoparticle Assemblies. ACS Applied Optical Materials 2024, 2 (10), 2118–2127.
- (19) Kaj, J.; Karam, P. Self-Referenced Temperature Sensor Based on Conjugated Polyelectrolytes. ACS Applied Polymer Materials 2024, 6 (12), 7036–7046.
- (20) Hassoun, S.; Karam, P. Fluorescent-Based Thermal Sensing in Lipid Membranes. *Langmuir* **2020**, *36* (5), 1221–1226.
- (21) Yassine, S. R.; Hassoun, S. A.; Karam, P. Fluorescent thermal sensing using conjugated polyelectrolytes in thin polymer films. *Anal. Chim. Acta* **2019**, *1077*, 249–254.
- (22) Ge, Y.; Duan, X.; Zhang, M.; Mei, L.; Hu, J.; Hu, W.; Duan, X. Direct room temperature welding and chemical protection of silver nanowire thin films for high performance transparent conductors. *J. Am. Chem. Soc.* **2018**, *140* (1), 193–199.
- (23) Hell, S. W.; Wichmann, J. Breaking the diffraction resolution limit by stimulated emission: stimulated-emission-depletion fluorescence microscopy. *Opt. Lett.* **1994**, *19* (11), 780–782.
- (24) Tan, C.; Pinto, M. R.; Schanze, K. S. Photophysics, aggregation and amplified quenching of a water-soluble poly (phenylene ethynylene). *Chem. Commun.* **2002**, 446–447.
- (25) Levitus, M.; Schmieder, K.; Ricks, H.; Shimizu, K. D.; Bunz, U. H.; Garcia-Garibay, M. A. Steps to demarcate the effects of chromophore aggregation and planarization in poly (phenyleneethynylene) s. 1. Rotationally interrupted conjugation in the excited states of 1, 4-bis (phenylethynyl) benzene. *J. Am. Chem. Soc.* **2001**, *123* (18), 4259–4265.
- (26) Walters, K. A.; Ley, K. D.; Schanze, K. S. Photophysical consequences of conformation and aggregation in dilute solutions of pi-conjugated oligomers. *Langmuir* 1999, 15, 5676–5680.
- (27) Zhao, X.; Jiang, H.; Schanze, K. S. Polymer chain length dependence of amplified fluorescence quenching in conjugated polyelectrolytes. *Macromolecules* **2008**, *41* (10), 3422–3428.
- (28) Kim, J.; Swager, T. M. Control of conformational and interpolymer effects in conjugated polymers. *Nature* **2001**, *411* (6841), 1030–1034.
- (29) Wang, Y.; Jones, E. M.; Tang, Y.; Ji, E.; Lopez, G. P.; Chi, E. Y.; Schanze, K. S.; Whitten, D. G. Effect of Polymer Chain Length on Membrane Perturbation Activity of Cationic Phenylene Ethynylene Oligomers and Polymers. *Langmuir* **2011**, *27* (17), 10770–10775.

- (30) Karam, P.; Hariri, A. A.; Calver, C. F.; Zhao, X.; Schanze, K. S.; Cosa, G. Interaction of Anionic Phenylene Ethynylene Polymers with Lipids: From Membrane Embedding to Liposome Fusion. *Langmuir* **2014**, *30* (35), 10704–10711.
- (31) Jiang, H.; Zhao, X.; Schanze, K. S. Amplified fluorescence quenching of a conjugated polyelectrolyte mediated by Ca2+. *Langmuir* **2006**, 22 (13), 5541–5543.
- (32) Yuan, X.; Xiang, T.-X.; Anderson, B. D.; Munson, E. J. Hydrogen bonding interactions in amorphous indomethacin and its amorphous solid dispersions with poly (vinylpyrrolidone) and poly (vinylpyrrolidone-co-vinyl acetate) studied using 13C solid-state NMR. *Mol. Pharmaceutics* **2015**, *12* (12), 4518–4528.
- (33) Lehmkemper, K.; Kyeremateng, S. O.; Heinzerling, O.; Degenhardt, M.; Sadowski, G. Long-Term Physical Stability of PVP- and PVPVA-Amorphous Solid Dispersions. *Mol. Pharmaceutics* **2017**, *14* (1), 157–171.
- (34) Darwish, G. H.; Abouzeid, J.; Karam, P. Tunable nanothermometer based on short poly (phenylene ethynylene). *RSC Adv.* **2016**, *6* (71), 67002–67010.
- (35) Yu, K.; Hodges, C.; Biggs, S.; Cayre, O. J.; Harbottle, D. Polymer molecular weight dependence on lubricating particle—Particle interactions. *Ind. Eng. Chem. Res.* **2018**, *57* (6), 2131–2138.
- (36) Zeng, X. M.; Martin, G. P.; Marriott, C. Effects of molecular weight of polyvinylpyrrolidone on the glass transition and crystallization of co-lyophilized sucrose. *International journal of pharmaceutics* **2001**, 218 (1–2), 63–73.
- (37) Benmore, C. J.; Benmore, S. R.; Wilke, S. K.; Menon, V.; Byrn, S. R.; Weber, J. K. R. X-ray Diffraction of Water in Polyvinylpyrrolidone. *Mol. Pharmaceutics* **2023**, 20 (7), 3645–3652.
- (38) Khataei, S.; H.Al-Musawi, M.; Asadi, K.; Ramezani, S.; Abbasian, M.; Ghorbani, M. Effect of molecular weight and content of polyvinylpyrrolidone on cell proliferation, loading capacity and properties of electrospun green tea essential oil-incorporated polyamide-6/polyvinylpyrrolidone nanofibers. *J. Drug Delivery Sci. Technol.* 2023, 82, No. 104310.
- (39) Schreiter, K. M.; Glawdel, T.; Forrest, J. A.; Ren, C. L. Robust thin-film fluorescence thermometry for prolonged measurements in microfluidic devices. *RSC Adv.* **2013**, 3 (38), 17236–17243.
- (40) Lee, J. H.; Chen, H.; Kim, E.; Zhang, H.; Wu, K.; Zhang, H.; Shen, X.; Zheng, Q.; Yang, J.; Jeon, S.; Kim, J. K. Flexible temperature sensors made of aligned electrospun carbon nanofiber films with outstanding sensitivity and selectivity towards temperature. *Materials Horizons* **2021**, *8* (5), 1488–1498.
- (41) Antić, Ż.; Dramićanin, M. D.; Prashanthi, K.; Jovanović, D.; Kuzman, S.; Thundat, T. Pulsed laser deposited dysprosium-doped gadolinium-vanadate thin films for noncontact, self-referencing luminescence thermometry. *Adv. Mater.* **2016**, 28 (35), 7745–7752.
- (42) Hua, Y.; Yu, J. S. Deep-red-emitting phosphors of Mn 4+-activated tantalite for high-sensitivity lifetime thermometry and security films. *Dalton Transactions* **2023**, *52* (31), 10751–10759.
- (43) Marin, R.; Millan, N. C.; Kelly, L.; Liu, N.; Rodrigues, E. M.; Murugesu, M.; Hemmer, E. Luminescence thermometry using sprayed films of metal complexes. *Journal of Materials Chemistry C* **2022**, *10* (5), 1767–1775.
- (44) He, S.; Mench, M. M.; Tadigadapa, S. Thin film temperature sensor for real-time measurement of electrolyte temperature in a polymer electrolyte fuel cell. *Sensors and Actuators A: Physical* **2006**, 125 (2), 170–177.
- (45) He, Z.; Yan, Y.; Zhang, Z. Thermal management and temperature uniformity enhancement of electronic devices by micro heat sinks: A review. *Energy* **2021**, *216*, No. 119223.
- (46) Mishra, D.; Hasrati, E.; Jain, A. Thermal management of Li-ion cells for improved safety and performance: a review. *Annual Review of Heat Transfer* **2023**, *26*, 131–176.
- (47) Trung, T. Q.; Duy, L. T.; Ramasundaram, S.; Lee, N.-E. Transparent, stretchable, and rapid-response humidity sensor for body-attachable wearable electronics. *Nano Research* **2017**, *10*, 2021–2033.

- (48) Agool, I.; Kadhim, K.; Hashim, A. Fabrication of new nanocomposites: (PVA-PEG-PVP) blend-zirconium oxide nanoparticles) for humidity sensors. *International Journal of Plastics Technology* **2017**, 21, 397–403.
- (49) Kumar, K.; Mehrotra, K.; Raj, A.; Pandey, S. P.; Bhattacharya, B. Humidity-Dependent Ion Conduction Mechanism of PVA-Based Polymer Electrolyte Films. *Macromol. Symp.* **2023**, *407*, 2100491.
- (50) Donato, N.; Aloisio, D.; Patti, E.; Latino, M.; Leonardi, S. G.; Spadaro, D. On the development and characterization of PMA-based SAW sensing devices. *Procedia Engineering* **2012**, 47, 1271–1274.
- (51) Park, S.-J.; Kim, M.-H.; Ha, T.-J. All-printed wearable humidity sensor with hydrophilic polyvinylpyrrolidone film for mobile respiration monitoring. *Sens. Actuators, B* **2023**, *394*, No. 134395.
- (52) Singh, P.; Saroj, A. Effect of ionic liquid on structural, thermal and electrical transport properties of PVA-PVP based polymer blend electrolyte membrane. *Phys. Scr.* **2021**, *96* (11), 115701.
- (53) Abe, S.; Chen, L. Tuning the photophysical properties of an ionic conjugated polymer through interactions with conventional polyelectrolytes. *J. Polym. Sci., Part B: Polym. Phys.* **2003**, *41* (14), 1676–1679.
- (54) Eder, T.; Stangl, T.; Gmelch, M.; Remmerssen, K.; Laux, D.; Höger, S.; Lupton, J. M.; Vogelsang, J. Switching between H- and J-type electronic coupling in single conjugated polymer aggregates. *Nat. Commun.* **2017**, *8* (1), 1641.
- (55) Ohira, A.; Swager, T. M. Ordering of poly (p-phenylene ethynylene) s in liquid crystals. *Macromolecules* **2007**, *40* (1), 19–25.
- (56) Jiang, X.; Wu, C.; Wohlgenannt, M.; Huang, W.; Kwei, T.; Okamoto, Y.; Vardeny, Z. Morphology-dependent optical properties of substituted poly (p-phenylene-ethynylene) (PPE) films. *Physica B: Condensed Matter* **2003**, 338 (1–4), 235–239.
- (57) Darwish, G. H.; Koubeissi, A.; Shoker, T.; Abou Shaheen, S.; Karam, P. Turning the heat on conjugated polyelectrolytes: an off—on ratiometric nanothermometer. *Chem. Commun.* **2016**, 52 (4), 823—826.
- (58) Kaj, J.; Hussein, D.; Karam, P. Fluorescent-Based Temperature Memory Reporter for Nanoscale Thermal Measurements. *J. Phys. Chem. C* **2022**, *126* (48), 20542–20549.
- (59) Levitsky, I. A.; Kim, J.; Swager, T. M. Energy Migration in a Poly (phenylene ethynylene): Determination of Interpolymer Transport in Anisotropic Langmuir— Blodgett Films. *J. Am. Chem. Soc.* **1999**, *121* (7), 1466–1472.
- (60) Moon, J. H.; Swager, T. M. Poly (p-phenylene ethynylene) brushes. *Macromolecules* **2002**, 35 (16), 6086–6089.
- (61) Deatsch, A. E.; Evans, B. A. Heating efficiency in magnetic nanoparticle hyperthermia. *J. Magn. Magn. Mater.* **2014**, 354, 163–172.
- (62) Yassine, S. R.; Fatfat, Z.; Darwish, G. H.; Karam, P. Localized catalysis driven by the induction heating of magnetic nanoparticles. *Catalysis Science & Technology* **2020**, *10* (12), 3890–3896.
- (63) Giustini, A. J.; Petryk, A. A.; Cassim, S. M.; Tate, J. A.; Baker, I.; Hoopes, P. J. Magnetic nanoparticle hyperthermia in cancer treatment. Nano. *Life* **2010**, *1* (01n02), 17–32.
- (64) Ganguly, S.; Margel, S. Design of magnetic hydrogels for hyperthermia and drug delivery. *Polymers* **2021**, *13* (23), 4259.
- (65) Guibert, C.; Dupuis, V.; Peyre, V.; Fresnais, J. Hyperthermia of Magnetic Nanoparticles: Experimental Study of the Role of Aggregation. J. Phys. Chem. C 2015, 119 (50), 28148–28154.
- (66) Zhao, X. Conjugated polyelectrolytes based on poly(arylene ethynylene): Synthesis, solution photophysics and applications to sensors and solar cells; University of Florida 2007.
- (67) Wehbe, M.; Kadah El Habbal, R.; Kaj, J.; Karam, P. Synergistic dual antibacterial activity of magnetite hydrogels doped with silver. *Langmuir* **2024**, *40* (43), 22865–22874.